

PAPER REF: 6719

PREDICTION OF AIR ENTRAPMENT DEFECT DURING ZINC ALLOY HIGH PRESSURE DIE CASTING BASED ON GAS-LIQUID MULTIPHASE FLOW MODEL

Liu Cao, Dunming Liao^(*), Fei Sun, Tao Chen, Zihao Teng, Yulong Tang

State Key Laboratory of Materials Processing and Die & Mould Technology, Huazhong University of Science and Technology (HUST), Wuhan, Hubei, China.

^(*)*Email: ldmhust73@163.com*

ABSTRACT

Zinc alloy is the preferred material for high pressure die casting (HPDC) production due to the good casting and mechanical properties, and the most common defect of zinc alloy die casting is air entrapment. A gas-liquid multiphase flow model is adopted to predict the gas entrapment defect during zinc alloy HPDC filling process, and the continuum surface force (CSF) model is used to treat the surface tension of gas-liquid multiphase. In addition, finite volume method (FVM) is adopted for discretization equations; the pressure implicit with splitting of operator (PISO) algorithm is adopted for coupling pressure and velocity; the volume of fluid (VOF) algorithm is adopted for interface tracking. A water filling experiment of an S-shaped channel is simulated, and the simulation results coincide well with the experiment results, which certifies the accuracy of the adopted model. Two HPDC filling processes of zinc alloy with different ingates are calculated, and the simulation results show that the gas entrapment defect with single ingate is obviously more than with double ingates, which coincide basically with the experiment results.

Keywords: gas-liquid multiphase flow, air entrapment, high pressure die casting, surface tension, finite volume method, numerical simulation.

INTRODUCTION

Zinc is one of the key developing metals in Chinese non-ferrous metal industry. Zinc alloy has many merits, such as the low melting point, and the high resistance to oxidation during melting, then the service life of the metal mould can be ensured; moreover, zinc alloy has good casting properties and can not adhere to the mould easily; meanwhile, zinc alloy has good deformation resistivity, high strength and abrasion resistance [1-3]. In the process of high pressure die casting (HPDC), the liquid metal fills the chamber with high speed and solidifies under pressure, so the production efficiency of HPDC is high and the product dimensional precision is well [4, 5]. The casting types of HPDC divide into hot and cold chamber die casting [6, 7]. Zinc alloy is widely used in the die casting products with thin wall and high demand of surface smoothness, and the casting type for zinc alloy is mainly hot chamber die casting [8]. The most common defect of zinc alloy die casting is air entrapment, which makes the metal structure loose and reduces the electric conductivity and strength, and the main source of the air entrapment defect is the gas entrapped during the filling process [9, 10]. Therefore, it is of great significance for zinc alloy HPDC production to predict the air entrapment defect accurately.

HPDC process has the characteristics of high filling speed and great interaction effect between gas and liquid metal. With the gradual improvement of numerical techniques, international and domestic scholars have done many researches deeply in the field of numerical simulation by HPDC [11-17]. Homayonifar et al. [18] calculated the air porosity distribution for HPDC based on the SOLA-VOF algorithm and a mixed VOF-Lagrange algorithm was developed in order to model splashing in HPDC, but the influence of gas phase during the filling process was not considered, such as the hindering effect of the isolated gas to the liquid metal. Zhao et al. [19] adopted direct finite difference method (DFDM) to describe the shape and location of free surfaces in casting mold filling processes, and the study indicates that final porosities in high pressure die castings are dependent on both gas entrapment during mold filling process and pressure transfer within solidification period. Ren et al. [20] simulated the filling processes of cool runner system and hot runner system by Flow-3D software, and the results show that using hot runner system in zinc die casting can reduce the loss of heat and pressure, save raw materials and improve quality as well as increase pattern yield. Cleary et al. [21] simulated HPDC process based on smoothed particle hydrodynamics (SPH) algorithm, which belongs to Lagrangian simulation techniques, and the results demonstrate that SPH simulations can be performed in reasonable computation times for large scale automotive castings and provide a high degree of predictive accuracy. Wu et al. [22] established a nucleation model that correlated the cooling rate with the nucleation density of magnesium alloys during solidification of HPDC process, and the model can also reveal the dendrite morphology with features of secondary and ternary dendrite branches. As seen from the relevant references, single-phase flow model is often applied in the simulation of HPDC filling process at present. In consideration of the great effect of gas phase to the HPDC filling process, gas-liquid multiphase flow model is of great value for simulating the HPDC filling process.

In the field of numerical simulation by casting process, finite difference method [23] (FDM), finite element method [24] (FEM) and finite volume method [25] (FVM) are the three most common numerical methods. FDM is easy to be implemented, while it's only suitable for structured mesh, causing that FDM can't fit complex surface boundary well [26]. FEM is appropriate for unstructured mesh and has a high calculation accuracy, but used for solving the thermal and stress field mainly [27]. FVM has the definite physical meaning and can be applied to unstructured mesh, and it is exercisable easily for FVM to discretize the governing equations, so FVM is widely used in computational fluid dynamics (CFD) [28]. The coupled solution of the pressure and velocity needs special handling in numerical modeling. Semi-implicit method for pressure-linked equations (SIMPLE) [29] algorithm and pressure implicit with splitting of operator (PISO) [30, 31] algorithm are widely adopted as the coupled solutions. SIMPLE algorithm is mainly used for steady flow, and PISO algorithm is mainly used for transient flow. One of the key techniques in two phase flow simulation is the interface tracking, which falls into two major categories: explicit interface tracking [32] and implicit interface tracking [33]. In the explicit interface tracking methods, the interface is tracked explicitly by mesh or particles, but the geometric topology change can not be handled well for the complex interface; in the implicit interface tracking methods, the interface is represented by the volume fraction of each elements, so it is fit for handling the complex geometric topology change and considering the effect of surface tension, and the volume of fluid (VOF) [34] algorithm is the most famous implicit interface tracking method. Taking the analysis above into consideration, synthesizing FVM for discretization governing equation, PISO for velocity-pressure coupling and VOF for interface tracking is appropriate for predicting the gas entrapment defect in zinc alloy HPDC process.

A gas-liquid multiphase flow model is used to handle the interaction effect between gas and liquid metal during zinc alloy HPDC filling process in this paper, and the surface tension of gas-liquid multiphase is also considered, then the gas entrapment defect of zinc alloy HPDC can be predicted accurately. FVM is adopted for discretization equations; PISO algorithm is adopted for coupling pressure and velocity; VOF algorithm is adopted for interface tracking. Through the work above, a fluid field numerical simulation program of HPDC based on gas-liquid multiphase flow model is developed. An S-shaped channel water filling experiment is simulated, and the simulation results are compared with the experiment results. Two HPDC filling processes of zinc alloy with different ingates are calculated, then the gas entrapment defects are compared according to the simulation and experiment results.

MATHEMATICAL AND NUMERICAL MODELING

(a) Governing Equations

The volume ratio α which represents the volume fraction of phase 1 at different locations, is adopted in VOF algorithm. The value 1 of α means that phase 1 completely occupies the location, and the value 0 means the contrary situation, so the value of α around the interface is between 0 and 1. The volume fraction equation which controls the distribution rule of α is:

$$\frac{\partial \alpha}{\partial t} + \nabla \cdot (\alpha \mathbf{U}) = 0 \quad (1)$$

According to the distribution of α , the unit normal vector \mathbf{n}_i at the interface can be calculated by:

$$\mathbf{n}_i = \frac{\nabla \alpha}{|\nabla \alpha|} \quad (2)$$

where the direction of \mathbf{n}_i is from phase 2 to phase 1. And then the curvature κ of the interface can be gotten by:

$$\kappa = -\nabla \cdot \mathbf{n}_i \quad (3)$$

The CSF [35] (continuum surface force) model is used to treat the surface tension of two phase flow in this paper, which can obtain the continuous pressure distribution, thereby the surface tension \mathbf{F}_σ at the interface can be obtained by:

$$\mathbf{F}_\sigma = C\kappa\nabla\alpha \quad (4)$$

Navier-Stokes equation [36] which is also called momentum equation, controls the change of \mathbf{U} :

$$\frac{\partial \rho \mathbf{U}}{\partial t} + \nabla \cdot (\rho \mathbf{U} \mathbf{U}) - \nabla \cdot \boldsymbol{\tau} = -\nabla p + \mathbf{S} \quad (5)$$

The definition of the mixed density ρ is:

$$\rho = \alpha_1 \rho_1 + \alpha_2 \rho_2 = \alpha_1 \rho_1 + (1 - \alpha_1) \rho_2 \quad (6)$$

Other physical parameters such as dynamic viscosity are also handled in the same way of ρ .

The source term \mathbf{S} can be expanded as below:

$$\mathbf{S} = \mathbf{F}_\sigma + \rho \mathbf{g} = C\kappa \nabla \alpha + \rho \mathbf{g} \quad (7)$$

The fluids in this paper are supposed to be incompressible, therefore the continuity equation which represents the mass conservation is:

$$\nabla \cdot \mathbf{U} = 0 \quad (8)$$

(b) Boundary conditions

By the above governing equations, in order to consider the influence of the gas to the liquid in the filling process of zinc alloy HPDC, the state motions of both the liquid and the gas are calculated in this paper. So the boundary conditions should be assigned on all boundaries. With regard to the HPDC process, the boundary types can be classified as inlet, outlet and wall.

For the inlet boundary, the volume fraction of phase 1 and the velocity are set artificially, and the pressure gradient is zero. For the outlet boundary, the pressure is set artificially, and the gradients of phase 1 volume fraction and the velocity are zero. For the wall boundary, the velocity boundary condition is no-slip, and the gradients of phase 1 volume fraction and the pressure are zero. The specific boundary conditions set in this paper are shown in Table 1.

Table 1 Boundary conditions

	inlet	outlet	wall
velocity	$\mathbf{U} = \mathbf{U}_{inlet}$	$\nabla U_x = \nabla U_y = \nabla U_z = \{0, 0, 0\}$	$\mathbf{U} = \{0, 0, 0\}$
pressure	$\nabla p = \{0, 0, 0\}$	$p = p_{outlet}$	$\nabla p = \{0, 0, 0\}$
volume fraction of phase 1	$\alpha = 1$	$\nabla \alpha = \{0, 0, 0\}$	$\nabla \alpha = \{0, 0, 0\}$

where the given pressure of the outlet p_{outlet} is usually set to the normal atmosphere or zero.

(c) Discretization equations and calculation methodology

The governing equations in this paper are discretized in the manner of FVM method. In the discretization process of FVM, volume integral of both equation ends are gained in terms of every control element, and corresponding interpolation operations are adopted, finally the solvable discrete equations can be obtained [25]. The volume integral of momentum equation is as below:

$$\int_{CV} \frac{\partial \rho \mathbf{U}}{\partial t} dV + \int_{CV} \nabla \cdot (\rho \mathbf{U} \mathbf{U}) dV - \int_{CV} \nabla \cdot \boldsymbol{\tau} dV = - \int_{CV} \nabla p dV + \int_{CV} \mathbf{S} dV \quad (9)$$

Gauss divergence theorem is a kind of transformation relation between volume integral and surface integral in vector field, as follows:

$$\int_{CV} \nabla \cdot \mathbf{F} dV = \int_A \mathbf{n} \cdot \mathbf{F}_f dA \quad (10)$$

By substituting Eq. (10) into Eq. (9), it can be acquired as below:

$$\int_{CV} \frac{\partial \rho U}{\partial t} dV + \int_A \mathbf{n} \cdot (\rho \mathbf{U} \mathbf{U})_f dA - \int_A \mathbf{n} \cdot \boldsymbol{\tau}_f dA = - \int_{CV} \nabla p dV + \int_{CV} \mathbf{S} dV \quad (11)$$

By reference to the relevant discretization operations in Ref. [25], such as the discretization formula for the diffusion term developed by Mathur [37], the higher-order differencing schemes for the convective term, and the co-located arrangement is used for velocity components and pressure. Then the discrete equations of momentum equation can be formulated as:

$$\mathbf{A}_p \mathbf{U}_P = \sum_N \mathbf{A}_N \mathbf{U}_N + \mathbf{B} + \sum_i \mathbf{A}_i p_i \quad (12)$$

According to Eq. (12), the velocity of the current control element P can be calculated by the velocity and pressure of the control elements contacting with P .

The volume integral of continuity equation is shown below:

$$\int_A \mathbf{n} \cdot \mathbf{U}_f = 0 \quad (13)$$

The face velocity \mathbf{U}_f is acquired by the interpolation scheme developed by Mathur [37], as follows:

$$\mathbf{U}_f = \left(\frac{\mathbf{U}_P + \mathbf{U}_N}{2} \right) \cdot \mathbf{n} + \frac{V_P + V_N}{A_P + A_N} \frac{1}{\xi_{PN}} \left(\frac{p_P - p_N}{2} + \frac{(\nabla p)_P + (\nabla p)_N}{2} \cdot \mathbf{e}_{PN} \right) \quad (14)$$

By substituting Eq. (14) into Eq. (13), the discrete equations of continuity equation can be formulated as:

$$\sum_i \mathbf{A}_{p,i} p_i = \mathbf{S}_p \quad (15)$$

According to Eq. (14) and Eq. (15), the continuity equation has been transformed into the pressure equation, by the special interpolation scheme for the face velocity. Further, the momentum equation and the continuity equation can be solved in a coupled solution.

Based on the discrete operations above, the discrete equation of the volume fraction equation can be obtained easily, as follows:

$$\sum_i \mathbf{A}_{\alpha,i} \alpha_i = \mathbf{S}_\alpha \quad (16)$$

PISO algorithm [30] is introduced into the coupled solution of the pressure and velocity in this paper, which is a non-iterative solution algorithm for transient flow, and the general calculation process of PISO is shown in Fig. 1.

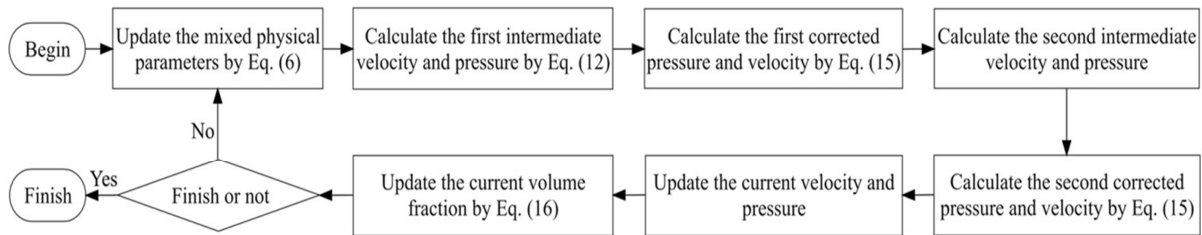


Fig. 1 - The general calculation process of PISO algorithm

RESULTS

According to the mathematical and numerical model above, the fluid field numerical simulation program of HPDC filling process based on gas-liquid multiphase model was developed in this paper. In order to verify the accuracy of the adopted model, an S-shaped channel water filling experiment is simulated, which was performed by Schmid [38], and the simulative results are compared with the experimental results. Then, two HPDC filling processes of zinc alloy with different ingates are calculated, and the gas entrapment defects are analyzed, which are also compared with the experimental results. In addition, the mesh generation tool used in this paper is ICEM CFD [39], and the open source software ParaView [40] is used for post-process.

(a) Filling of an S-shaped channel

The water experiment was performed on a cold chamber die-casting machine [41, 42], and the inner chamber is a horizontal S-shaped channel. The geometric dimension of the S-shaped channel is shown in Fig. 2, and the thickness of the channel is 2 mm. The valve which is shown in the top of Fig. 2 is designed to be very small, so the gas entrapment phenomena can be observed obviously during water filling. The inlet velocity is designed to be 8.7 m/s, which is very high compared to typical filling process. Table 2 contains the parameters needed in the simulation.

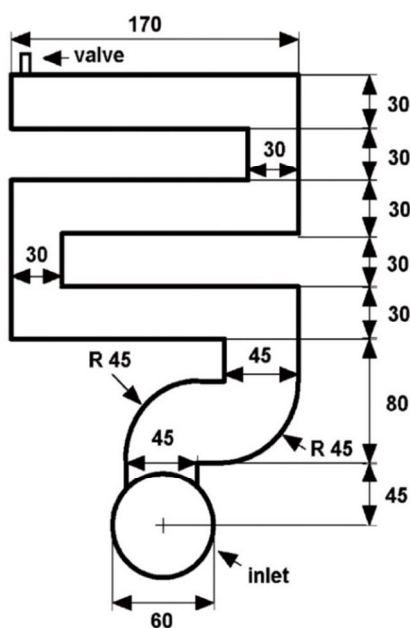


Fig. 2 - The geometric dimension of the S-shaped channel (unit: mm)

Table 2 The parameters needed in the simulation of the S-shaped channel

parameter	value
water density (kg/m^3)	1000
air density (kg/m^3)	1
water dynamic viscosity ($\text{Pa}\cdot\text{s}$)	1e-3
air dynamic viscosity ($\text{Pa}\cdot\text{s}$)	1e-5
water-air surface tension coefficient (N/m)	0.07275
acceleration of gravity (m/s^2)	{0,0 - 9,8}
inlet velocity (m/s)	{0,8 - 7,0}
outlet pressure (Pa)	0

The comparison between the experimental results and the simulative results are shown in Fig. 3, and the simulative results include the distributions of water volume fraction and gas-liquid velocity. As seen from the comparison results, at 7.15 ms, the water flow had a sharp front under the influence of the curved inlet in experiment, which the simulative results corresponds with well; at 25.03 ms, a big gas bubble existed at the low right in both the experimental and simulative results; at 39.34 ms, the water flow began to touch the upper right wall in both the experimental and simulative results, and the bubble at the low right became smaller; at 53.64 ms, the water front reached the valve, and the distribution of water flow basically coincided between the experimental and simulative results. Moreover, the air was driven strongly by the water flow in the filling process, according to the distribution of gas-liquid velocity. In consequence, the accuracy of the adopted model is certified well for simulating high speed filling process by the comparison results.

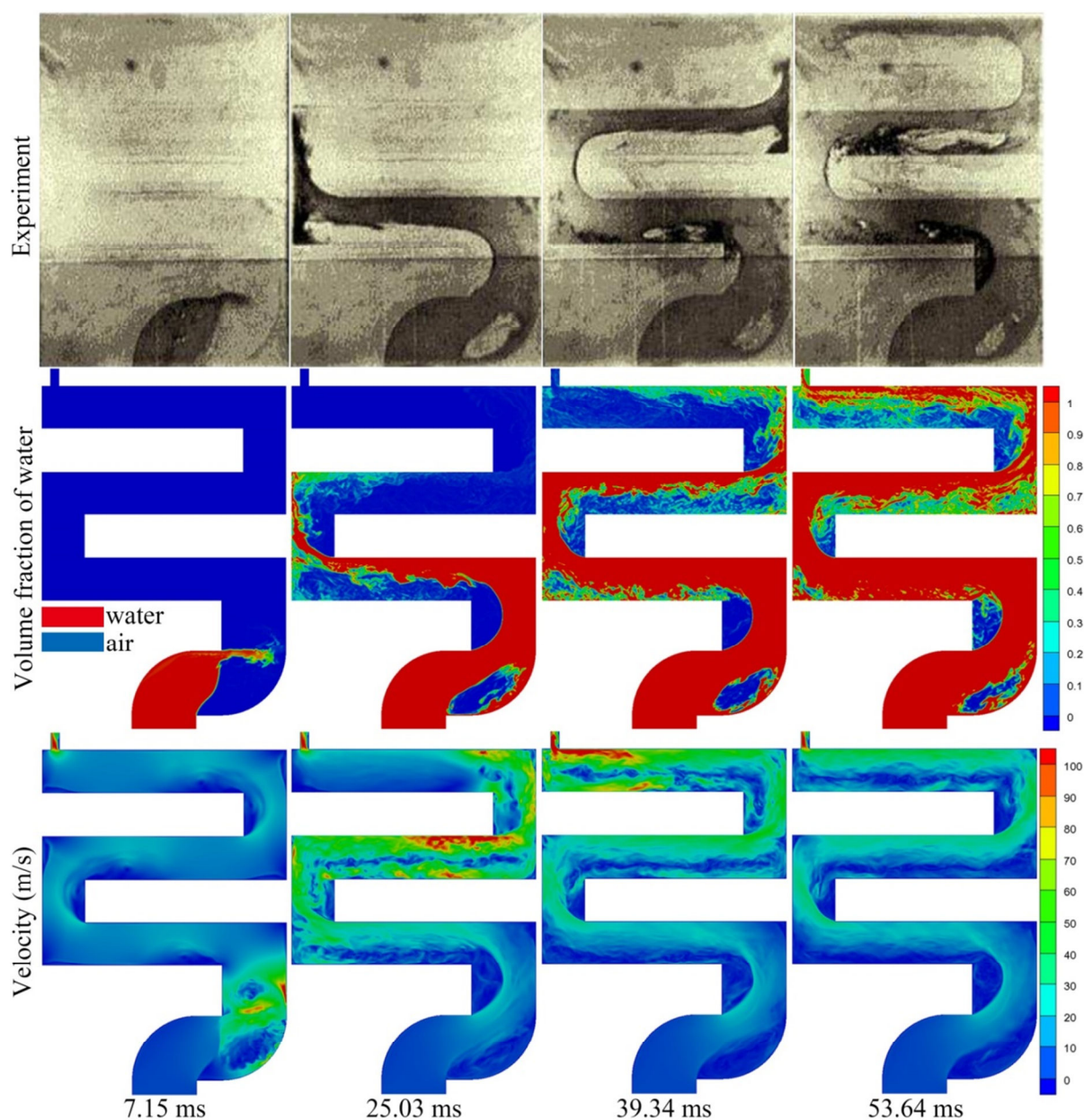


Fig. 3 - The comparison between the experimental results and the simulative results of S-shaped channel filling

(b) Geometric model of zinc alloy HPDC and parameters setting

For the sake of analyzing the gas entrapment defect in zinc alloy HPDC filling process, two schemes with different ingates were designed in this paper. Figure 4 shows the geometric model and mesh of scheme 1 and scheme 2, and the locations of inlet and outlet are marked in Fig. 4. In scheme 1, the inlet with single ingate locates the bottom of the casting; In scheme 2, the inlet with double ingates locate the left and right sides of the casting. The overall dimensions of the casting is 112×28×18 mm.

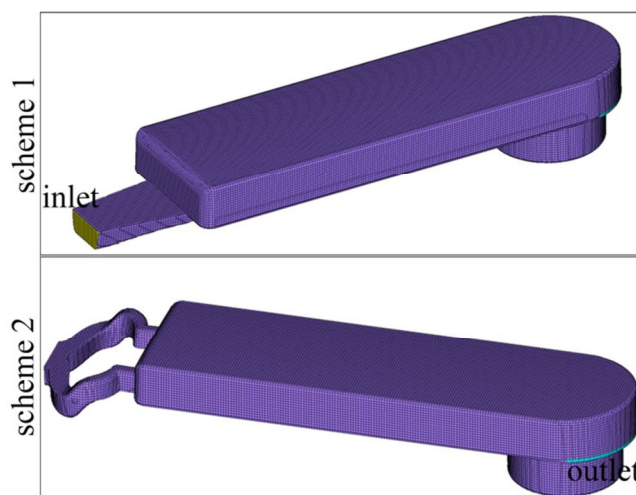


Fig. 4 - The geometric model and mesh of scheme 1 and scheme 2

The zinc alloy material used in the experiment is Zamak3, the chemical compositions of which are 95.87% Zn, 4.00% Al, 0.03% Mg, 0.10% Cu. Table 3 contains the parameters needed in the simulation.

Table 3 - The parameters needed in the simulation of zinc alloy HPDC filling

parameter	value
zinc alloy density (kg/m ³)	6300
air density (kg/m ³)	1
zinc alloy dynamic viscosity (Pa·s)	0.05
air dynamic viscosity (Pa·s)	1e-5
zinc alloy-air surface tension coefficient (N/m)	0.0782
acceleration of gravity (m/s ²)	{0, 0, -9.8}
inlet velocity (m/s)	{3.5, 0, 0}
outlet pressure (Pa)	0

Before analyzing the simulative and experimental results, it is necessary to firstly introduce the heat treatment method of the casting in this paper. Heat treatment is unfit for the traditional die castings, for the reason that the metal strength reduces after heating, and the gas entrapped during the filling process expands by heating, thus convex bubbles can be observed with ease on the casting surface. Making use of this phenomenon, the die castings were heated, so as to intuitively observe the gas entrapment defect. The specific craft of heat treatment in this paper is temperature (350 °C) and time (3 hours, not contain the time of heating up). The effects of the zinc alloy castings after heating are shown in Fig. 5, and the expanded bubbles after heating are inside the red wireframes.

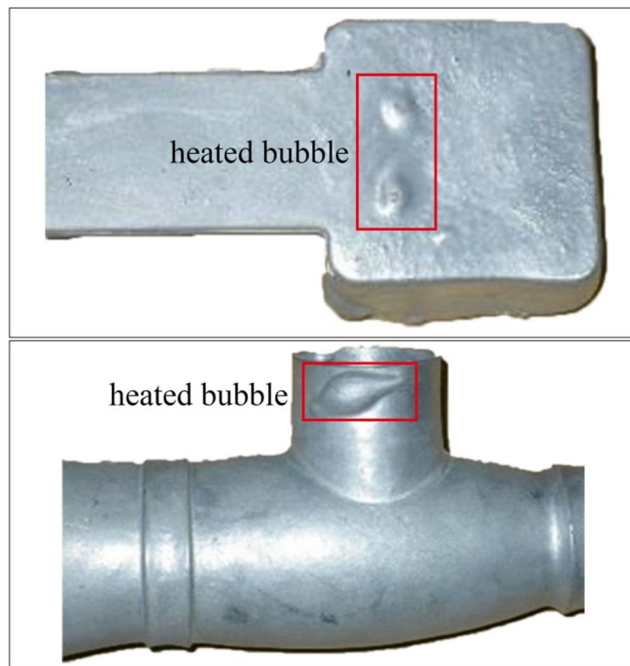


Fig. 5 - The effects of the zinc alloy castings by heat treatment

(c) Comparison and analyses for simulation and experiment results

Figure 6 shows the liquid volume fraction and velocity of scheme 1 and scheme 2 after filling 0.015 s. From the comparison results, in scheme 1, the velocity of the liquid flow was high when entering the chamber and the direction was up-inclined, because the ingate is on the bottom and the cross section area of the ingate gradually lessens, and the liquid front flowed along the upper wall after touching the upper wall; in scheme 2, the direction of the liquid flow was horizontally forward, because of the double ingates located the left and right sides of the casting. Therefore, a big closed gas region appeared on the upper left of the casting in scheme 1, by reason of the up-inclined liquid flow, and the gas phase distributions of scheme 1 and scheme 2 after filling 0.055 s are shown in Fig. 7. As seen from Fig. 7, in scheme 1, a mount of gas was entrapped in the left during the filling process, although the entrapped gas could move forward gradually with the liquid flow, but it was very easy to form tiny gas entrapment defect; in scheme 2, most of the gas phase moved towards the outlet.

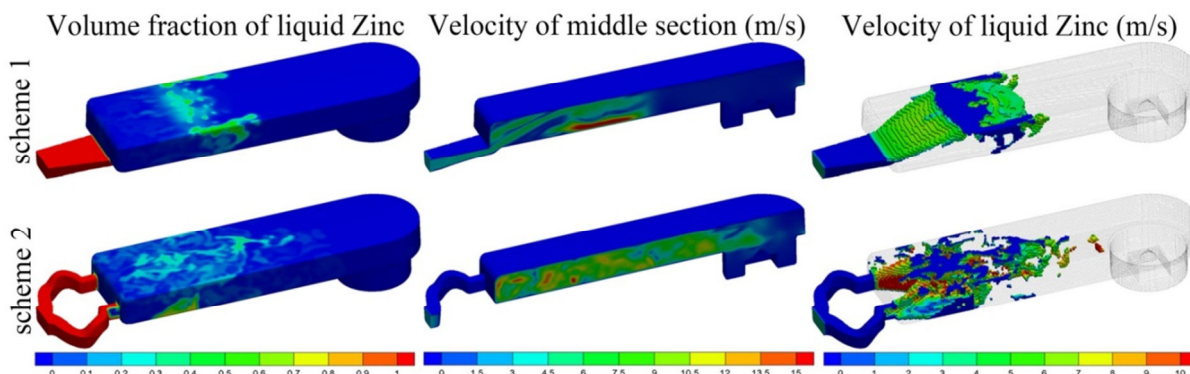


Fig. 6 - The liquid volume fraction and velocity of scheme 1 and scheme 2 after filling 0.015 s

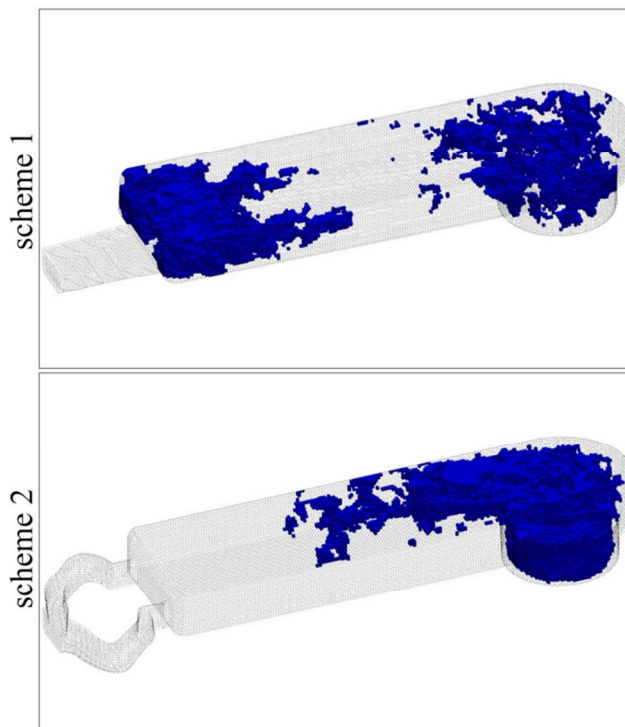


Fig. 7 - The gas phase distributions of scheme 1 and scheme 2 after filling 0.055 s

Figure 8 shows the experiment results of scheme 1 and scheme 2 including the zinc alloy die castings and the heated castings, and the simulation results of the final zinc alloy distributions. By the comparison of the die castings of scheme 1 and scheme 2, the surfaces of the die castings were smooth, so it is most unlikely to distinguish the gas entrapment defect by sight. From the comparison of the heated castings of scheme 1 and scheme 2, it is obvious that a lot of gas distributed on the middle and outlet end of the casting in scheme 1, and there was only a handful of gas on the outlet end of the casting in scheme 2. By the comparison of the simulation results of the final zinc alloy distributions, more gas existed on the middle and outlet end of the casting in scheme 1, and bits of gas concentrated on the outlet end of the casting in scheme 2. As seen from the comparison results, the simulation and experiment results agree basically for the gas entrapment defect.



Fig. 8 - The experiment results of scheme 1 and scheme 2 including the zinc alloy die castings and the heated castings, and the simulation results of the final zinc alloy distributions

CONCLUSIONS

- 1) A gas-liquid multiphase flow model is adopted to predict the gas entrapment defect during zinc alloy HPDC filling process, and the fluid field numerical simulation program is developed in this paper. In addition, FVM is adopted for discretization equations; PISO algorithm is adopted for coupling pressure and velocity; VOF algorithm is adopted for interface tracking;
- 2) The CSF model is used to treat the surface tension of gas-liquid phase, so the interaction effect of gas-liquid phase can be considered accurately;
- 3) A water filling experiment of an S-shaped channel is simulated, and the simulation results coincide well with the experiment results, which certifies the accuracy of the adopted model;
- 4) Two HPDC filling processes of zinc alloy with different ingates are calculated, and the gas entrapment defects are compared according to the simulation and experiment results, which coincide basically with each other.

ACKNOWLEDGMENTS

This research is financially supported by the Program for New Century Excellent Talents in University (No. NCET-13-0229, NCET-09-0396), the National Science & Technology Key Projects of Numerical Control (No. 2012ZX04010-031, 2012ZX0412-011) and the National High Technology Research and Development Program (“863” Program) of China (No. 2013031003).

REFERENCES

- [1]-Xue T, Gu W Q, Yu Y F et al (2016) Research and Application Development in Die Casting Zinc Alloy. *Special Casting & Nonferrous Alloys* 36(3):260-264
- [2]-Ritchie I G, Pan Z L, Goodwin F E (1991) Characterization of the damping properties of die-cast zinc-aluminum alloys. *Metall Mater Trans A* 22(3):617-622
- [3]-Gervais E, Barnhurst R J, Loong C A (1985) An analysis of selected properties of ZA alloys. *Jom* 37(11):43-47
- [4]-Chiang K T, Liu N M, Tsai T C (2009) Modeling and analysis of the effects of processing parameters on the performance characteristics in the high pressure die casting process of Al-Si alloys. *Int J Adv Manuf Technol* 41(11-12):1076-1084
- [5]-Kong L X, She F H, Gao W M et al (2008) Integrated optimization system for high pressure die casting processes. *J Mater Process Tech* 201(1):629-634
- [6]-Okayasu M, Yoshifuji S, Mizuno M et al (2009) Comparison of mechanical properties of die cast aluminium alloys: cold v. hot chamber die casting and high v. low speed filling die casting. *Int J Cast Metal Res* 22(5):374-381

- [7]-Tang J Q (2015) Application of Hot Runner to Hot Chamber Die Casting Production. Foundry 64(5):409-414
- [8]-Apelian D, Paliwal M, Herrschaft D C (1981) Casting with zinc alloys. Jom 33(11):12-20
- [9]-Shen J N (2013) Study of Numerical Simulation and Hot Runner Technology for Zinc Alloy Die Casting. Dissertation, Jimei University
- [10]-Lai Z W (2012) Study on the Blow Hole Defect Cause of Formation and Countermeasures in Miniature Ultrathin Zinc Alloy Die Castings. Dissertation, Tsinghua University
- [11]-Verran G O, Mendes R P K, Rossi M A (2006) Influence of injection parameters on defects formation in die casting Al12Si1, 3Cu alloy: Experimental results and numeric simulation. J Mater Process Tech 179(1):190-195
- [12]-Hu B H, Tong K K, Niu X P et al (2000) Design and optimisation of runner and gating systems for the die casting of thin-walled magnesium telecommunication parts through numerical simulation. J Mater Process Tech 105(1):128-133
- [13]-Long A, Thornhill D, Armstrong C et al (2011) Determination of the heat transfer coefficient at the metal-die interface for high pressure die cast AlSi9Cu3Fe. Appl Therm Eng 31(17):3996-4006
- [14]-Jia L R, Xiong S M, Feng W M et al (2001) Numerical simulation of fluid flow and heat transfer during mold filling for die casting. Journal of Tsinghua University 41(2):8-11
- [15]-Helenius R, Lohne O, Arnberg L et al (2005) The heat transfer during filling of a high-pressure die-casting shot sleeve. Mat Sci Eng A 413:52-55
- [16]-Cleary P W, Ha J, Ahuja V (2000) High pressure die casting simulation using smoothed particle hydrodynamics. Int J Cast Metal Res 12(6):335-356
- [17]-Ha J, Cleary P W (2000) Comparison of SPH simulations of high pressure die casting with the experiments and VOF simulations of Schmid and Klein. Int J Cast Metal Res 12(6):409-418
- [18]-Homayonifar P, Babaei R, Attar E et al (2008) Numerical modeling of splashing and air entrapment in high-pressure die casting. Int J Adv Manuf Technol 39(3-4):219-228
- [19]-Zhao H D, Bai Y F, Ouyang X X et al (2010) Simulation of mold filling and prediction of gas entrapment on practical high pressure die castings. T Nonferr Metal Soc 20(11):2064-2070
- [20]-Ren L X, Shen J N, Que F B et al (2014) Study on Die-Casting Hot Runner System for Zinc Alloy Based on Numerical Simulation. Hot Working Technology 43(7):61-64
- [21]-Cleary P W, Ha J, Prakash M et al (2006) 3D SPH flow predictions and validation for high pressure die casting of automotive components. Appl Math Model 30(11):1406-1427

- [22]-Wu M W, Xiong S M (2010) Microstructure simulation of high pressure die cast magnesium alloy based on modified CA method. *Acta Metall Sin* 46(12):1534-1542
- [23]-Mitchell A R, Griffiths D F (1980) *The finite difference method in partial differential equations*. John Wiley & Sons, Hoboken
- [24]-Dhatt G, Lefrançois E, Touzot G (2012) *Finite Element Method*. John Wiley & Sons, Hoboken
- [25]-Versteeg H K, Malalasekera W (2007) *An introduction to computational fluid dynamics: the finite volume method*. Pearson Education, New York
- [26]-Vladimir G (2009) Finite-difference methods for simulating the solidification of castings. *Materials in technology* 43(5):233-237
- [27]-Cao L, Liao D, Lu Y Z et al (2016) Heat Transfer Model of Directional Solidification by LMC Process for Superalloy Casting Based on Finite Element Method. *Metall Mater Trans A* 47(9):4640-4647
- [28]-Kim J, Kim D, Choi H (2001) An immersed-boundary finite-volume method for simulations of flow in complex geometries. *J Comput Phys* 171(1):132-150
- [29]-Patankar S V, Spalding D B (1972) A calculation procedure for heat, mass and momentum transfer in three-dimensional parabolic flows. *Int J Heat Mass Tran* 15(10):1787-1806
- [30]-Issa R I, Gosman A D, Watkins A P (1986) The computation of compressible and incompressible recirculating flows by a non-iterative implicit scheme. *J Comput Phys* 62(1):66-82
- [31]-Park T S (2006) Effects of Time-Integration Method in a Large-Eddy Simulation Using the PISO Algorithm: Part I—Flow Field. *Numer Heat Tr A-Appl* 50(3):229-245
- [32]-Bridson R, Houriham J, Nordenstam M (2007) Curl-noise for procedural fluid flow. *Acm T Graphic* 26(3):46
- [33]-Hirt C W, Nichols B D (1981) Volume of fluid (VOF) method for the dynamics of free boundaries. *J Comput Phys* 39(1):201-225
- [34]-Ménard T, Tanguy S, Berlemont A (2007) Coupling level set/VOF/ghost fluid methods: Validation and application to 3D simulation of the primary break-up of a liquid jet. *Int J Multiphas Flow* 33(5):510-524
- [35]-Brackbill J U, Kothe D B, Zemach C (1992) A continuum method for modeling surface tension. *J Comput Phys* 100(2):335-354
- [36]-Constantin P, Foias C (1988) *Navier-stokes equations*. University of Chicago Press, Chicago.
- [37]-Mathur S R, Murthy J Y (1997) Pressure boundary conditions for incompressible flow using unstructured meshes. *Numer Heat Tr B-Fund* 32(3):283-298

[38]-Schmid M, Klein F (1995) Fluid flow in die cavities-experimental and numerical simulation, NADCA 18. International Die Casting Congress and Exposition

[39]-Xu L, Luo H X (2008) The Technology of Numerical Simulation Based on ANSYS ICEM CFD and CFX Software. Mechanical Engineer 12:65-66

[40]-Henderson A, Ahrens J, Law C (2004) The ParaView Guide. Kitware, New York

[41]-Tavakoli R, Babaei R, Varahram N et al (2006) Numerical simulation of liquid/gas phase flow during mold filling. Comput Method Appl M 196(1):697-713

[42]-Pang S, Chen L L, Zhang M Y et al (2010) Numerical simulation two phase flows of casting filling process using SOLA particle level set method. Appl Math Model 34(12):4106-4122.